Journal of Molecular Liquids 343 (2021) 117636

Contents lists available at ScienceDirect

Journal of Molecular Liquids

journal homepage: www.elsevier.com/locate/molliq

# The hydrophobic core effect in model bacterial membranes upon interaction with tetra-*p*-guanidinoethylcalix[4]arene

Beata Korchowiec [a,*], Monika Orlof-Naturalna [a,b], Jacek Korchowiec [a], Jean-Bernard Regnouf de Vains [c], Maxime Mourer [c], Ewa Rogalska [c,*]

[a] Faculty of Chemistry, Jagiellonian University, ul. Gronostajowa 2, 30-387 Krakow, Poland
[b] Faculty of Civil Engineering and Resource Management, AGH University of Science and Technology, ul. A. Mickiewicza 30, 30-059 Krakow, Poland
[c] Université de Lorraine, CNRS, L2CM, F-5400 Nancy, France

ARTICLE INFO

*Article history:*
Received 8 July 2021
Revised 13 September 2021
Accepted 19 September 2021
Available online 22 September 2021

*Keywords:*
Drug-membrane interaction
Calixarene
Membrane penetration
Antibacterials
Molecular modeling

ABSTRACT

The calixarene derivative used in this study (tetra-*p*-guanidinoethylcalix[4]arene) shows in vitro activity against different Gram-positive and Gram-negative bacteria. The interaction between bacterial cell membranes and the water-soluble calixarene was investigated using model lipids spread as monomolecular films at the air–water interface. Compression and adsorption experiments, as well as Brewster angle microscopy, polarization modulation-infrared reflection–absorption spectroscopy and computer modeling permitted understanding of the intra- and intermolecular interaction in several lipid-calixarene systems. Because the affinity of the calixarene derivative for the membranes may be linked to the interaction with negative charges, phosphatidylglycerols were used as model lipids; the phosphatidylglycerols contained saturated or unsaturated hydrocarbon chains with different lengths. It was showed that the affinity of the calixarene for the monolayer depends on the structure of the phosphatidylglycerols side chains. This observation may be of interest for a further development of new antibiotics.


## 1. Introduction

New effective antibiotics with precise antimicrobial and cell-penetrating activities are urgently needed to address the mounting resistance challenge. Calixarenes are considered as versatile platforms for synthesizing bioactive agents [1]. These organic macrocyclic molecules contain a series of phenolic units linked through methylene bridges at the *ortho*-position to the hydroxyl group present on the aromatic moiety [2]. It was shown in the literature that different calixarene derivatives interact with lipid bilayers and modify their properties [3]. This observation is important for engineering molecular structures with an affinity towards bacterial membrane.

Among different calix[4]arene derivatives synthesized in our group, some have antibacterial properties [4–6]. This is the case of the derivative CX1 (Scheme 1) which is amphiphilic due to four hydrophilic *p*-ethylguanidinium groups grafted on the upper rim of the calixarene annulus [7–9]. The impact of CX1 on bacterial membranes was observed in vitro using microscopy [10], electrophoretic mobility [10], and membrane permeability measurements [11]. The disruption of bacterial membranes could be explained in terms of an interplay between electrostatic and nonelectrostatic interactions between the calixarene and the membrane, as reported in the case of antibacterial peptides [12]. On the other hand, it can be supposed that the composition of the membrane lipids in bacteria is important for the interaction with third molecules [13]. The results obtained in our previous studies showed that CX1 behaves differently relative to zwitterionic phosphoglycerides or those bearing a negative charge in the polar head [14,15]. Indeed, a clear difference was observed between monomolecular films formed with the negatively charged DMPG or DMPS compared to the neutral DMPC or DMPE; the effect of CX1 on the model bacterial membranes used in this study was more important in the former case. The results obtained showed the importance of the concurrent charge-charge and apolar interaction between CX1 and phospholipids forming the film and indicate that this effect may play a role in the antibacterial activity of different molecules.

It must be kept in mind that cell membranes are fluid structures. Because fluidity is essential for membrane function, living organisms can adjust it in response to physical, chemical or biological stimuli. Changes in unsaturated fatty acid ratios in response to stress was described in the case of plants [16]. Similarly, the levels

* Corresponding authors.
*E-mail address:* bkorch@chemia.uj.edu.pl (B. Korchowiec).

https://doi.org/10.1016/j.molliq.2021.117636
0167-7322/

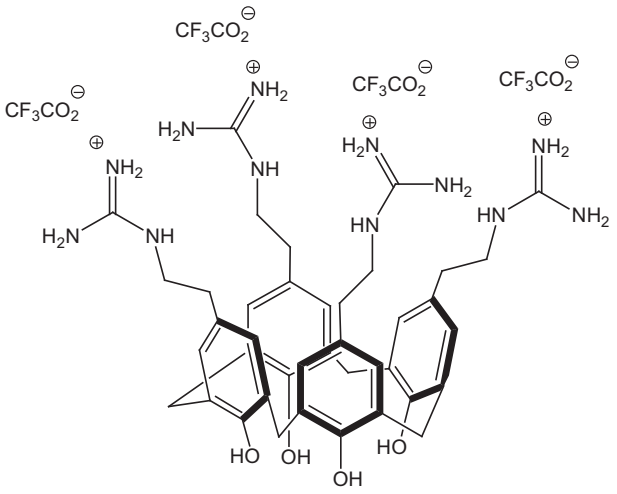

**Scheme 1.** The tetra-*p*-guanidinoethylcalix[4]arene trifluoroacetate salt (CX1) structure.

of unsaturated, branched and short-chain fatty acids can be changed in bacteria [17]. It was proposed recently that this phenomenon can be a decisive factor in the mechanism of membrane-targeting antibiotics [18–22]. Information on membrane structure and its physico-chemical properties is thus important to understand antibiotic mechanisms [18,19,22,23]. For example, some antibiotics can perturb the cell wall biogenesis machinery anchored in the fluid microdomains of bacterial lipid membranes [19,22]. Fluidity measurements can be performed using lipophilic fluorescent stains, namely Laurdan and DiIC12 [23].

Langmuir films showed to be useful in elucidating different biological events [24]. Here, monomolecular films formed with model bacterial phospholipids were used to study the role of membrane fluidity in the interaction with CX1 [25–30]. In the present study, monomolecular films formed with negatively charged phospholipids, namely phosphatidylglycerols were used as model bacterial membranes. The saturated or unsaturated lipids with different chain length or saturation allowed assessing the effect of CX1 depending on film fluidity.

The results obtained with surface pressure-area ($\Pi$–$A$) compression isotherms, Brewster angle microscopy (BAM), polarization modulation-infrared reflection–absorption spectroscopy (PM-IRRAS) and molecular modeling monolayers showed a significant difference between the medium and long chain, as well as saturated and unsaturated chain phosphoglycerides upon interaction with CX1.

## 2. Materials and methods

### 2.1. Materials

The chemical structure of the calixarene derivative used in this study is presented in Scheme 1. The synthesis of this compound was published before [7]. Synthetic DLPG, DMPG, DPPG, DSPG, and DOPG (sodium salts, Avanti Polar Lipids; ~99.9% pure) and chloroform (Sigma-Aldrich; purity ~ 99.9%) were used to prepare the phospholipid solutions. An aqueous solution of CX1 with a concentration of 4.0 mg $L^{-1}$ was used as the subphase. This concentration was found to be the minimum inhibitory concentration (MIC) for CX1 in *E. coli*. At the concentration of CX1 used, no surface activity of the calixarene derivative is observed. MilliQ water was used in all experiments (resistivity of 18.2 MΩ·cm at 25 °C; surface tension of 72.8 mN $m^{-1}$ at 20 °C, pH 5.6).

### 2.2. Surface pressure isotherms and Brewster angle microscopy

A KSV 2000 Langmuir balance with a Wilhelmy plate and a Teflon® trough (58 × 15 × 1 cm) with two hydrophilic Delrin barriers were used for surface pressure ($\Pi$) measurements. Phospholipid chloroform solutions with precise concentrations were used to form monolayers with a Hamilton microsyringe on the top of aqueous subphases. After 20 min, the monolayers were compressed symmetrically at a rate of 2.5 mm·$min^{-1}$ per barrier. The isotherm measurements were repeated three times. The accuracy of the results was ± 0.1 $Å^2$ for the mean molecular area and ± 0.01 mN·$m^{-1}$ for surface pressure measurements. The experiments were performed at 20 °C.

Compression isotherms ($\Pi$–$A$) allowed for determination of the compressibility modulus: $C_s^{-1} = -A(d\Pi/dA)_T$ [31].

The morphology of the monolayers was imaged using a computer-linked KSV 2000 Langmuir balance connected to a Brewster angle microscope (KSV Optrel BAM 300). The dimensions of the Teflon® trough were 58 × 6.5 × 1 cm; the other experimental conditions were as described above.

### 2.3. Adsorption kinetics measurement

A 20 mL Teflon® dish with pure water was used for the adsorption experiments. The phospholipid solutions were spread at the air–water interface using a Hamilton microsyringe and a small volume of concentrated aqueous CX1 solution was injected into the subphase through the film. The final concentration of CX1 in the subphase was the same as in the case of compression isotherms. Surface pressure changes were monitored using a KSV 2000 Langmuir balance. All measurements were carried out at 20 °C.

### 2.4. Polarization modulation – infrared reflection – absorption spectroscopy (PM-IRRAS)

A KSV PMI 550 instrument was used for PM-IRRAS measurements. The PM-IRRAS spectra of phospholipid films spread on pure water or 4.0 mg $L^{-1}$ CX1 aqueous solution were recorded at 20 °C. Monolayers were prepared as described in Section 2.2. The parameters and operating principle of the PMI 550 spectrometer were as published before [29].

### 2.5. Computational details

The symmetric model of water-air interface was applied. Each monolayer contained 100 lipid molecules. The anionic phospholipids were neutralized by sodium cations. Two types of calculations were performed to study the effect of CX1 cation, neutralized by chloride anions, on the lipid monolayer. In the first, preliminary type of calculations, a single CX1 moiety was placed 20 Å below the upper lipid layer. The equilibrated lipid monolayers were taken to build the initial configurations. The area per lipid was set to 80 $Å^2$. This value corresponds to liquid expanded state of the monolayer. After short 0.5 ns run, the potential mean force (PMF) calculations [32] were performed. The difference between *z*-coordinates of center of mass of CX1 cation and center of mass the water slab was chosen as "reaction" coordinate. The reaction coordinate was divided into 2.5 Å length intervals. Each interval was probed for 0.5 ns. Such choice of interval length guarantee that the whole interval was equally populated. In the second type of calculations, the water soluble CX1 cations were placed 20 Å below (above) the upper (the lower) water slab surface (*xy* cut), respectively, and distributed on a 2D lattice (3 × 3 grid). CX1 cations were

randomly oriented. Again, the equilibrated lipid monolayers were taken to build these models. The value of area per lipid was the same as in PMF calculations. Canonical ensemble calculations (*NVT*, number of particles, volume, temperature) were performed at $T$ = 20 °C. The second type of calculations were carried out for 120 ns. Periodic boundary conditions were imposed. Translational replicas in *z*-direction were separated by "vacuum" slab to minimize the mutual interaction among monolayers in this direction. The last 24 ns of each simulation were used for further analysis.

Molecular dynamics simulations were carried out using the NAMD package [33]. The collvar technique of NAMD was applied to carry on potential mean force calculations [32,34]. The CHARMM all atom force-field [35,36] and TIP3P [37] water model were employed. Langevin thermostat with a damping parameter equal to 5 ps was applied. Van der Waals interactions were disregarded for mutual separation higher than 1.2 nm; to omit discontinuity the potential was smoothed starting at 1.0 nm. Long-range electrostatic interactions were computed by the particle-mesh Ewald algorithm [38].

## 3. Results and discussion

### 3.1. Compression and adsorption isotherms

The compression isotherms and the compressibility modulus - surface pressure ($C_s^{-1}-\Pi$) dependencies obtained with the monolayers formed with five phosphoglycerols bearing different lateral chains are presented in Fig. 1. The physicochemical properties of the monolayers spread on pure water differ significantly. The compressibility of the films [31] decreases in the order: DLPG, DOPG, DMPG, DPPG and DSPG (Table 1). In the case of DMPG, a phase transition liquid expanded – liquid condensed is observed.

The isotherms obtained on the CX1 solution are shifted to higher molecular areas compared to pure water (Fig. 1b). The profiles of the isotherms corresponding to DLPG, DMPG, DOPG and DPPG are similar up to 45 mN·m$^{-1}$; DSPG differs from the other four films, as it shows a plateau at 30 mN·m$^{-1}$. The compressibility of DMPG, DPPG and DSPG is significantly lower in the presence of CX1 compared to pure water while that of the more liquid-like DLPG and DOPG is not much altered (Fig. 1b, inset). Interestingly, the $C_s^{-1}-\Pi$ curves are superposed during almost whole compression cycle in the case of DLPG, DMPG, DOPG and DPPG, while for DSPG it decreases abruptly at around 28 mN·m$^{-1}$ and then increases upon further compression to the values close to those of the pure DSPG. It can be said that CX1 interacts with all phosphoglycerols used in this study, as indicated by the increase of both the molecular area and the compressibility of the monolayers. It can be observed that this effect is the least important in the case of the unsaturated DOPG. The relatively low shift of the DOPG isotherm may suggest that the interaction with CX1 is different compared to the other lipids. In the case of DMPG, the BAM images (Fig. 2) show that the characteristic phase transition disappears in the presence of CX1.

This result is in accordance with the compression isotherm experiments and indicates that CX1 is present in the DMPG monolayer at the surface pressure corresponding to the phase transition.

As proposed in our precedent studies [14], mixed films are formed with CX1 and negatively charged phospholipids via a complex interplay of charge-charge and apolar interaction. However, it can be supposed that the interaction depends as well on the structure of the lipid side chains. With the aim to better understand this point, the experiments of adsorption of CX1 to phosphoglycerol films were performed. The kinetics of CX1 adsorption to monolayers formed with each of the five phosphoglycerols are shown in Fig. 3. The initial surface pressure of the films was 30 mN m$^{-1}$ this value is considered as corresponding to the pressure in the biological cell membranes [39].

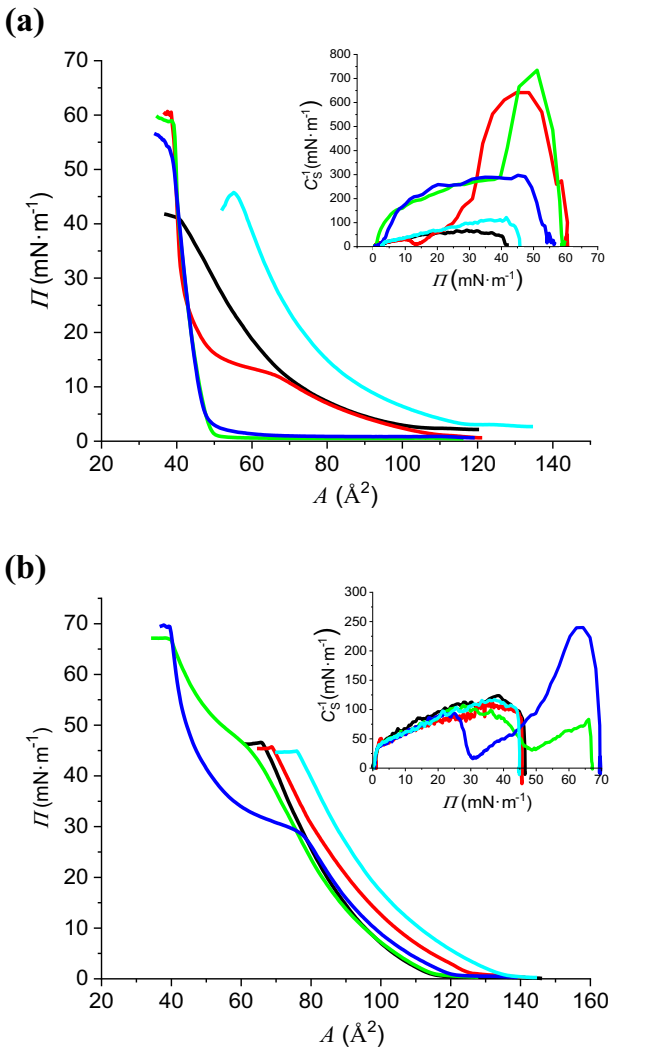


**Fig. 1.** Surface pressure isotherms of phospholipid films formed on pure water (a) and on 4.0 mg L$^{-1}$ CX1 solution (b). Results obtained with DLPG (black), DMPG (red), DPPG (green), DSPG (blue) and DOPG (cyan); Temperature: 20 °C. Insets: $C_s^{-1}-\Pi$ dependency. (For interpretation of the references to color in this figure legend, the reader is referred to the web version of this article.)

**Table 1**
Characteristic parameters of isotherms at $\Pi$ = 30 mN m$^{-1}$.

| | $A$ (Å$^2$) | $C_s^{-1}$ (mN m$^{-1}$) |
|---|---|---|
| DLPG/water | 49.8 | 63.2 |
| DLPG/CX1 solution | 77.1 | 118.2 |
| DMPG/water | 41.7 | 181.8 |
| DMPG/CX1 solution | 80.5 | 95.5 |
| DPPG/water | 42.1 | 274.1 |
| DPPG/CX1 solution | 75.3 | 97.4 |
| DSPG/water | 42.3 | 279.4 |
| DSPG/CX1 solution | 73.3 | 18.8 |
| DOPG/water | 65.1 | 106.8 |
| DOPG/CX1 solution | 87.0 | 102.7 |

It can be observed that in the case of DOPG, DLPG and DMPG the value of the equilibrium surface pressure ($\Pi_{eq}$; 43, 47 and 46 mN m$^{-1}$, respectively; measured 60 min after injection) corresponds to the collapse of the Langmuir films pinpointed as the maximum of $C_s^{-1}$ (Fig. 1b inset). In the case of DSPG and DPPG, the $\Pi_{eq}$ values

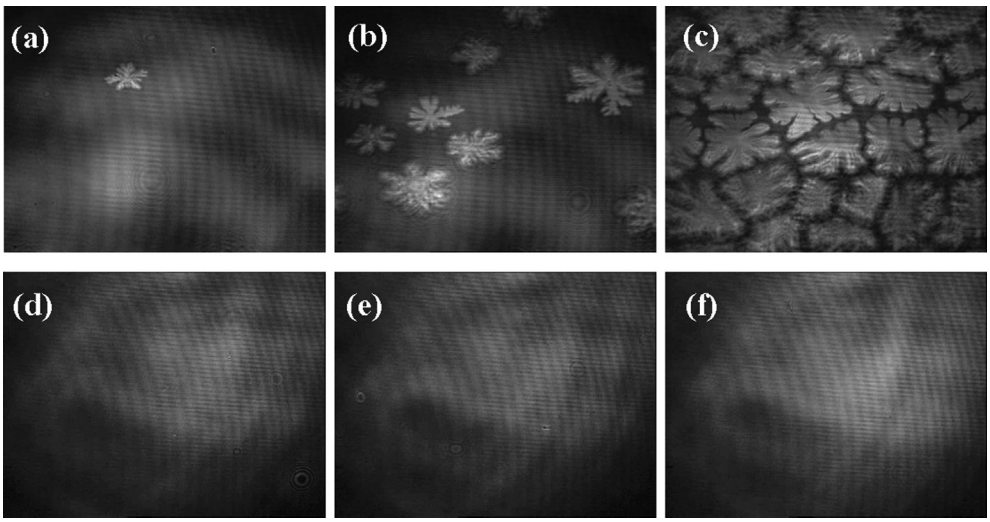


**Fig. 2.** BAM micrographs of DMPG monolayers. Line a-c: DMPG on pure water at 68 (a), 60 (b) and 48 Å$^2$ (c); line d-f: DMPG on 4 mg L$^{-1}$ CX1 solution at 95 (d), 90 (e) and 80 Å$^2$ (f). Scale: the width of the images corresponds to 345 μm.

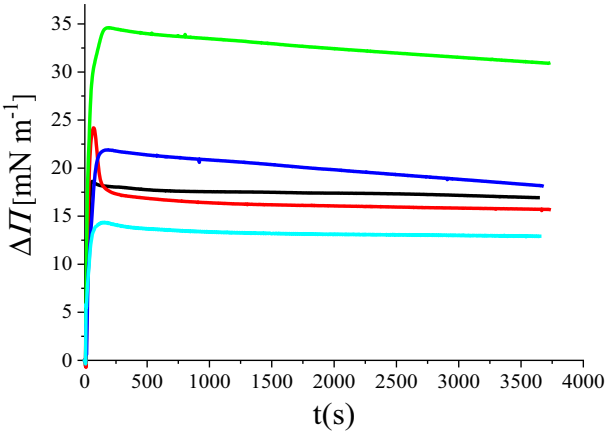


**Fig. 3.** Adsorption kinetics of CX1 to DLPG (black), DMPG (red), DPPG (green), DSPG (blue), and DOPG (cyan) monolayers. The initial surface pressure, $\Pi_0$ = 30 mN m$^{-1}$ was normalized to 0. The concentration of CX1 in the subphase was 4 mg·L$^{-1}$. (For interpretation of the references to color in this figure legend, the reader is referred to the web version of this article.)

(48 and 60 mN m$^{-1}$, respectively) correspond to the condensed monolayers formed upon compression at the molecular area of around 45 Å$^2$ (Fig. 1b). These results suggest that in the latter two lipids, the interaction with CX1 is modified upon compression. Based on the compression and the adsorption experiments we propose that below 30 mN m$^{-1}$ CX1 is intercalated between the DSPG molecules [14]. Above this value it would be progressively expulsed below the polar heads. The same process would take place with DPPG above 40 mN m$^{-1}$. In the case of DLPG and DMPG, CX1 would be intercalated between the lipids at all surface pressures.

### 3.2. Polarization modulation – infrared reflection – absorption spectroscopy

The PM-IRRAS spectra obtained with DLPG, DMPG, DPPG, DSPG or DOPG monolayers are presented in Fig. A1 of Supplementary Material. The monolayers were formed on a pure water subphase or on the CX1 solution. The spectra were registered at $\Pi$ = 30 mN·m$^{-1}$. To get more insight in the reorganization of the monolayers in the presence of CX1, the DPPG and DSPG spectra were registered at $\Pi$ = 60 mN·m$^{-1}$ as well (Fig. A1, green line). The CX1 impact on phospholipid monolayers was analyzed by comparing stretching vibrations of methylene and carbonyl groups of phospholipids in the case of pure water subphase and CX1 solution (Table 2).

The $CH_2$ stretching vibrations allow determining the conformation of the phospholipid side chains. In the case of the monolayers formed with the long chain phospholipids (DPPG and DSPG) on pure water, the characteristic vibrations show at wavenumbers 2920 cm$^{-1}$ and 2850 cm$^{-1}$, or lower. This result indicates that the chains adopt *trans* conformation in the monolayer. In the case of the shorter chains (DLPG and DMPG), the $CH_2$ frequencies appear at higher values (blueshift). This observation indicates that the DLPG and DMPG chains adopt *gauche* conformation in the monolayers. Consequently, the chains are less ordered, and the monolayers are more liquid-like compared to DPPG or DSPG. The most important shift of the $CH_2$ signals to higher frequencies is observed in the case of the DOPG monolayer. This observation is in accordance with the compression isotherm results indicating the lowest ordering of the unsaturated chains and the most liquid-like character of the DOPG monolayer compared to the other lipids used.

The PM-IRRAS results obtained on the CX1 subphase show that the calixarene derivative interacts and has an impact on the order-

**Table 2**
Methylene and carbonyl stretching vibrations of phospholipids in the absence and presence of CX1 at 30 and 60 mN.m$^{-1}$.

| | $\nu_{as}(CH_2)$ (cm$^{-1}$) | $\nu_s(CH_2)$ (cm$^{-1}$) | $\nu$(C=O) (cm$^{-1}$) |
|---|---|---|---|
| DLPG/water | 2923 | 2853 | 1748 |
| DLPG/CX1 solution | 2931 | 2859 | 1739, 1750 |
| DMPG/water | 2920 | 2851 | 1747 |
| DMPG/CX1 solution | 2930 | 2858 | 1739, 1749 |
| DPPG/water | 2919 | 2850 | 1743 |
| DPPG/CX1 solution | 2928 | 2855 | 1737, 1748 |
| (*)DPPG/CX1 solution | 2922 | 2855 | 1744 |
| DSPG/water | 2918 | 2849 | 1740 |
| DSPG/CX1 solution | 2927 | 2854 | 1737, 1746 |
| (*)DSPG/CX1 solution | 2922 | 2853 | 1742 |
| DOPG/water | 2926 | 2859 | 1749 |
| DOPG/CX1 solution | 2931 | 2862 | 1741, 1756 |

(*) $\Pi$ = 60 mN·m$^{-1}$.

ing of the lipids, as reflected by the $\nu_{as}(CH_2)$ and $\nu_s(CH_2)$ shifts. A blueshift of $\nu_{as}(CH_2)$ and $\nu_s(CH_2)$ compared with pure water results from chain disordering and an increase of conformational liberty [40,41]. This effect, i.e. decrease of chain ordering (more *gauche* conformers) and liquefaction of the monolayer is the least pronounced in the case of DOPG. The latter may indicate less interaction of CX1 with the unsaturated lipid chain.

The bands observed at approx. 1730 $cm^{-1}$ can be attributed to the C=O stretching vibrations of the lipids. Importantly, the position of ν(C=O) is sensitive to hydrogen bonding and, consequently, to hydration of the polar groups. A redshift (shift to lower wavenumbers) indicates hydration, while a blueshift indicates dehydration of the C=O groups due to reduced water availability [42,43]. On the pure water subphase, the lower ν(C=O) values observed with the DPPG or DSPG monolayers compared to DLPG, DMPG or DOPG suggest that the polar heads in the long chain lipids are more hydrated compared to the shorter or unsaturated chain lipids. This effect indicates a higher ordering of the more rigid, long and saturated chains via a higher number of hydrogen bonding network [44,45].

The signal obtained in the presence of CX1 were deconvoluted into two ν(C=O) bands which were assigned to the *sn*-1 and *sn*-2 carbonyl groups of the lipid [42,46,47]. As can be seen in Table 2, the *sn*-1 C=O groups are slightly dehydrated while the *sn*-2 C=O groups are highly hydrated in all lipids, showing the red shift of the second band, compared to the single band observed with the pure water subphase. This suggests that the chemical environment of *sn*-1 C=O groups is almost unchanged in the presence of CX1, while the availability of water for *sn*-2 C=O groups increases. This may be due to the displacement of the $Na^+$ cation from the polar head to the subphase and binding of guanidinium groups to the anionic phosphate group in lipids [14]. Splitting of the signals observed with the CX1 solution may indicate coexistence of CX1-bound and CX1-free lipids in the monolayer.

Interestingly, the PM-IRRAS spectra obtained with DPPG or DSPG on the CX1 subphase at $\Pi$=60 $mN{\cdot}m^{-1}$ reveal a single ν (C=O) peak. This peak is only slightly (approx. 2 $cm^{-1}$) blueshifted compared to pure water, indicating comparable hydration of the lipid polar heads with the two subphases. On the other hand, the blueshift of the corresponding $CH_2$ bands observed at 60 $mN{\cdot}m^{-1}$ is significantly lower compared to that at 30 $mN{\cdot}m^{-1}$. These outcomes are in accordance with the compression isotherm results and indicate that CX1 is removed from the DPPG and DSPG monolayers at high surface pressures.

### 3.3. MD simulations

The interaction of CX1 with lipid monolayer was probed using modelling. The results illustrating preliminary calculations, namely the change in free energy along the reaction coordinate, are shown in Fig. 4. The curves present $\Delta F$ corresponding to the most stable configuration, different for each molecular system. Therefore, all curves have minima at $\Delta F$ = 0 kcal $mol^{-1}$. These points represent the adsorption of CX1 to the monolayer with the calixarene crown immersed in water. The curves indicate that penetration of CX1 to the DOPG monolayer is the least favorable process; the penetration into the DLPG monolayer has a lower free energy cost. None of the curve points correspond to the presence of the CX1 crown in the hydrophobic lipid chain region. The latter result is in accordance with the flip-flop mechanism of the CX1 penetration to anionic monolayers described previously [14]. The PMF calculations are long-term and were performed to capture the qualitative difference related to the penetration of CX1 cations into monolayers composed of lipids with the same head groups. The flip-flop adsorption mechanism involves much longer simulations and this issue is discussed in the second type of our simulations.

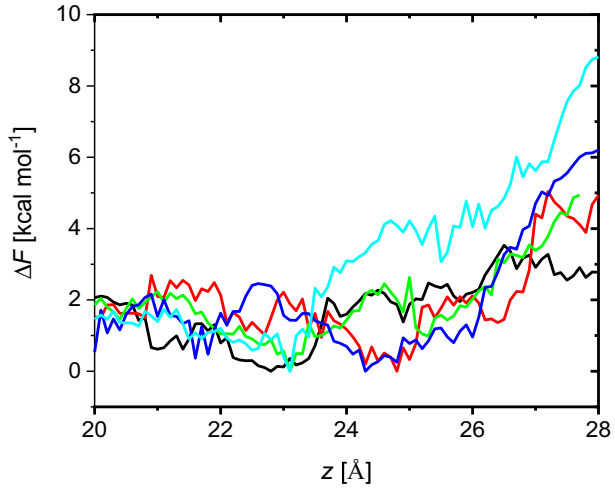


**Fig. 4.** Free energy change along the reaction coordinate (difference between the *z* coordinates of the center of mass of the CX1 cation and the center of mass of the water slab). Color code: DLPG (black); DMPG (red); DPPG (green); DSPG (blue); DOPG (cyan). (For interpretation of the references to color in this figure legend, the reader is referred to the web version of this article.)

Representative snapshots (last frame of the 120 ns simulation run), showing side views of the lipid monolayers with CX1, are presented in Fig. 5. For reasons of clarity, hydrogen atoms in phospholipid molecules were excluded from the figure. The image was plotted by using VMD graphics package. It can be seen that CX1 cations accumulate close to the monolayers. This effect can be attributed to the electrostatic attraction between the negatively charged head groups and the CX1 cations. Two coordination patterns can be distinguished, the first with calixarene crowns immersed in water, and the second with calixarene crowns located in the hydrophobic part of phospholipid monolayers. The shorter the lipids tails, the more CX1 molecules are transferred to the hydrophobic tail region. The transfer of the CX1 cation to the tail region is associated with the flip-flop movement of the calixarene crown [14]. In order to minimize unfavorable electrostatic interactions, the crown is rotated 180° along the *x* or *y* axis with simultaneous vertical transfer towards the tail. This behavior of the CX1 cation keeps the guanidinium groups immersed in water.

It should be noted that the transfer occurs with different efficiency depending on the structure of the hydrophobic tail. For example, three CX1 cations can be observed in the DLPG tail region and only one in the case of DSPG. Importantly, there are no CX1 cations in the tail region of the DOPG monolayer. Another observation from the image is the decrease in the order of the chains in the immediate vicinity of the CX1 cations. This is especially well seen with longer chains (see Fig. 5c and d).

The observations resulting from the single simulation frame shown in Fig. 5 were confirmed by the partial density plots depicted in Fig. 6. The plots were obtained by averaging 24 ns trajectories. The distribution of lipid $CH_3$ groups in DLPG/CX1 and DMPG/CX1 systems is broad and symmetrical compared to pure monolayers at high surface pressure. This indicates a relatively large freedom in the orientation of the lipid chains. The asymmetry in the density profile of the $CH_3$ groups should indicate an increase in order (carbon atoms in *trans* configuration). The maxima of the $PO_4$ and OH groups of the lipid and $NH_2$ of the CX1 are located in approximately the same region at the interface. The partial density plots of calixarene OH, with the exception of DOPG/CX1 system, have two distinct regions indicating two modes of coordination as illustrated in Fig. 6. In Fig. 6f the partial density plots are superposed and enlarged to show more clearly the penetration of the

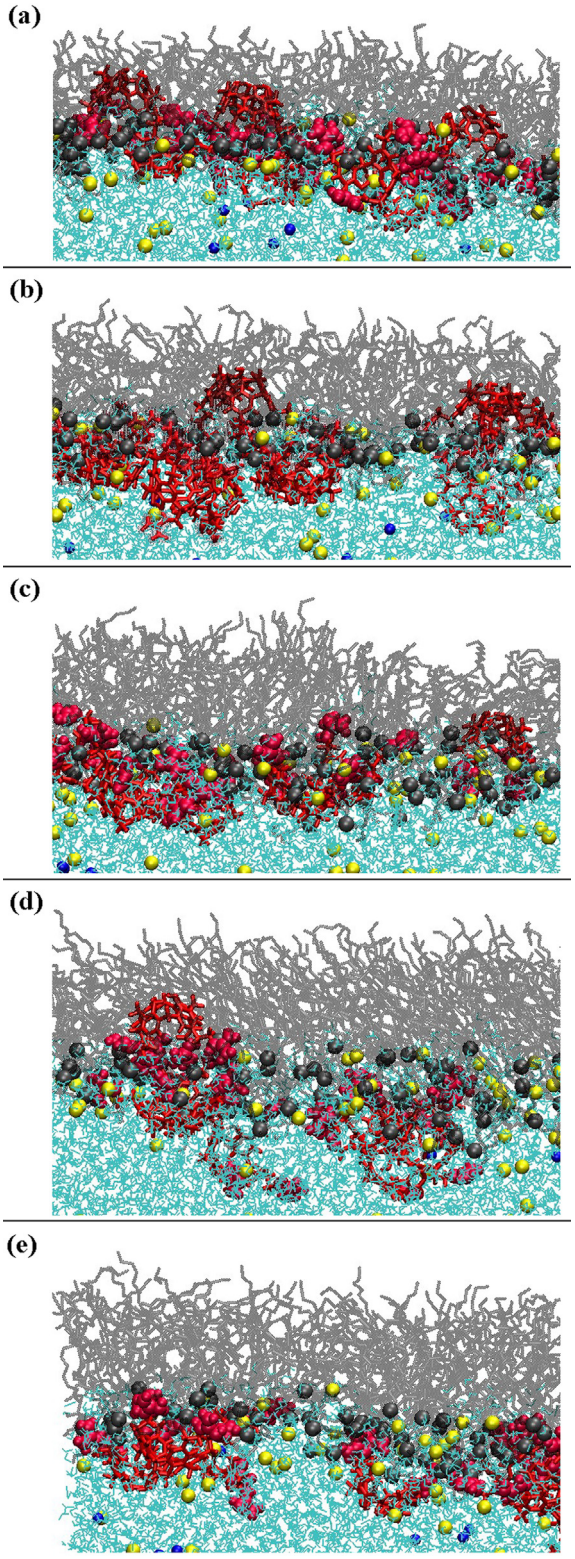


**Fig. 5.** Side views of lipid monolayers containing CX1. Only the upper monolayers are shown: (a) DLPG/CX1, (b) DMPG/CX1, (c) DPPG/CX1, (d) DSPG/CX1, and (e) DOPG/CX1. Red sticks: CX1 cations; red balls: guanidinium groups; gray sticks: phospholipids; gray balls: lipid phosphorous atoms; yellow balls: $Na^+$; blue balls: $Cl^-$; cyan: water molecules. (For interpretation of the references to color in this figure legend, the reader is referred to the web version of this article.)

calixarene crowns. In the case of the DOPG monolayer, only one maximum is visible. Thus, the CX1 cation did not penetrate into the tail region. This behavior clearly distinguishes DOPG bearing two unsaturated chains from the other four, saturated phospholipids. This was also reflected in the adsorption kinetics plot in Fig. 3. A similar phenomenon was observed in the model lung surfactant monolayer [48], in which unsaturated *sn*-2 chains of POPC formed a roof over benzo[a]pyrene molecules and thus constituted a barrier to the penetration of these molecules into the monolayer.

The hydrophilic parts of the monolayers can be characterized by the hydration/coordination numbers, $n_c$, which can be computed by integrating the radial distribution function to a first minimum. The data obtained in this way are summarized in Table 3. The dependence of the distance of $n_c = n_c(r)$ is illustrated in Fig. A2 of Supplementary Material.

The phosphoryl and carbonyl oxygen atoms are less hydrated in DLPG/CX1, DMPG/CX1, DPPG/CX1, DSPG/CX1 and DOPG/CX1 compared to pure DLPG, DMPG, DPPG, DSPG, and DOPG monolayers, respectively. The effect is much stronger for the phosphoryl than carbonyl oxygen atoms. Similar conclusions concern coordination of sodium ions. Data related to the guanidinium hydrogen atoms ($H_G$) clearly show formation of strong hydrogen bonds with $O_P$ (see also Fig. A2). The affinity of $H_G$ for $O_P$ is approximately 5–6 times greater than for $O_C$. These findings confirm the strong affinity of CX1 ions for anionic monolayers [14]. The lower hydration numbers of $O_C$ due to CX1 adsorption to the monolayer show as well in the PM-IRRAS data, namely the blueshift of the stretching vibration ν(C═O). It is worth noting that the simulations were carried out at a constant area while the experimental data were collected at constant pressure. Constant pressure simulation should enhance the above observations related to the coordination numbers.

Almost all molecular systems analyzed at the lipid surface area of 80 $Å^2$ correspond to the liquid expanded state of the film. The latter is in accordance with the surface pressure isotherms presented in Fig. 1b. The presence of CX1, except the DSPG/CX1 case, does not change the phase behavior. In the DSPG/CX1 monolayer, an area of 80 $Å^2$ corresponds to the beginning of the isotherm plateau. The tilt angle probability distribution and the average dihedral angles along the *sn*-2 hydrocarbon chain are shown in Fig. 7a and b, respectively. The qualitative behavior of the *sn*-1 chain is analogous to the *sn*-2 chain and is presented in Fig. A3.

The tilt angle of the hydrocarbon chain is defined by the angle between the vector coming from C-2 and going to C-*M* (*M* = 12, 14, 16, 18, 18 for DLPG, DMPG, DPPG, DSPG, DOPG, respectively), and the normal to the surface. The height and the width, as well as the position of the maximum of the tilt angle probability distribution remain almost unchanged when the CX1 cations are added to the solution. The only difference can be observed between the DSPG and DSPG/CX1 systems. The latter monolayer is more ordered, as indicated by a narrower curve and with the maximum higher compared to the other curves. Similar conclusions can be drawn from Fig. 7b. The curves showing the average dihedral angles along the *sn*-2 chains are almost identical for the three pairs of systems: DLPG/CX1 and DLPG, DMPG/CX1 and DMPG, DPPG/CX1 and DPPG. However, an important difference is seen for the DSPG/CX1 and pure DSPG compared to the other lipids, as in the latter case CX1 has an ordering effect. The longer the unsaturated chain, the greater the dihedral angle. The collapse of the curve observed in the DOPG/CX1 and DOPG systems is related to the double bond. The change in hybridization at two carbon atoms imposes a value for the dihedral angle (zero for the conformer *cis*). It also reduces ordering in the immediate vicinity of this angle.

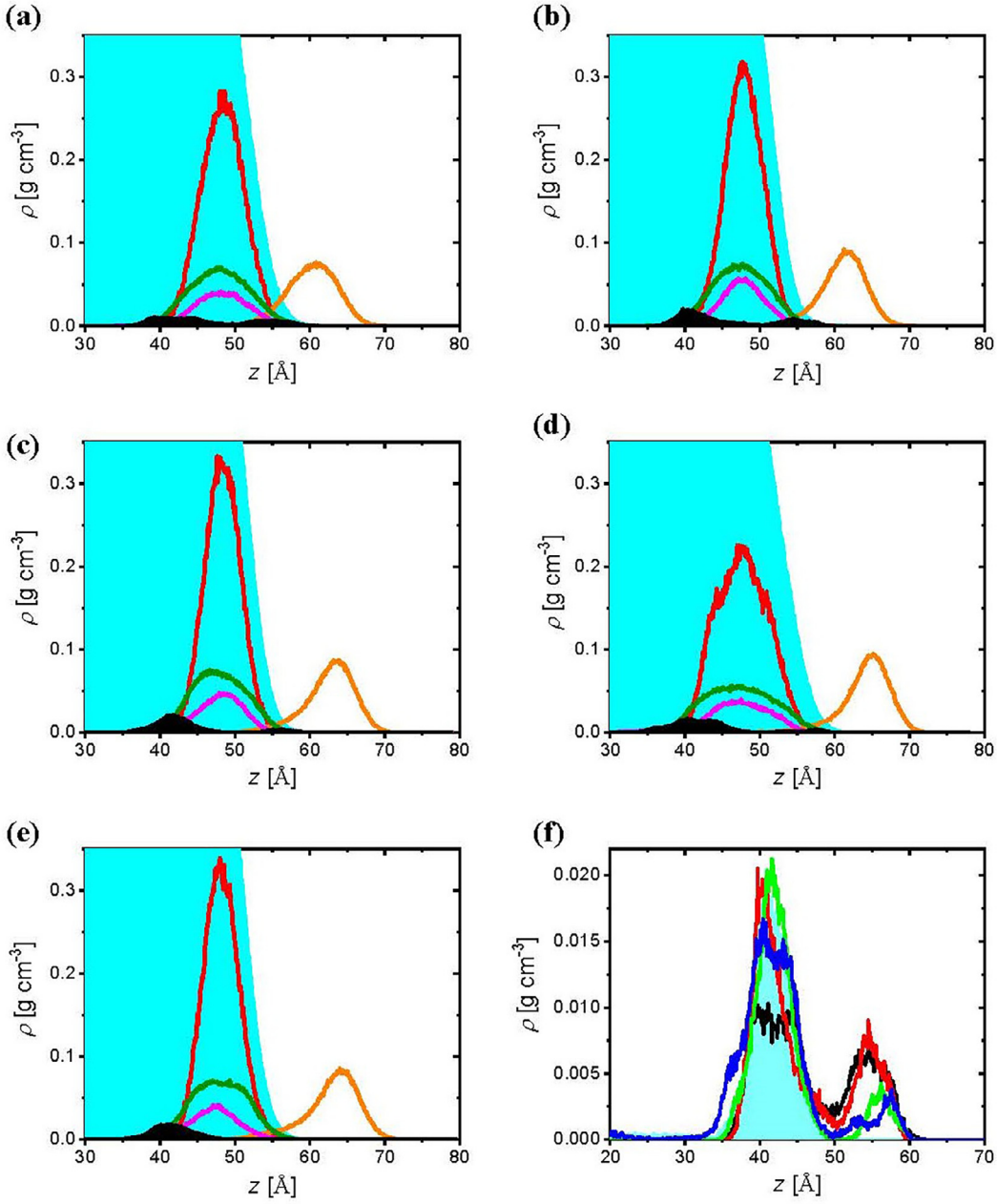


**Fig. 6.** Partial density profiles, $\rho_X = \rho_X(z)$, of DLPG (a), DMPG (b), DPPG (c), DSPG (d) and DOPG (e), respectively. Cyan: $X$ = $H_2O$; red: $X$ = $PO_4^-$; orange: $X$ = $CH_3$; magenta: $X$ = OH of lipid, green: $X$ = $NH_2$ of CX1; black: OH in CX1. Panel (f) corresponds to the partial density plots of OH in CX1; black line: DLPG; red line: DMPG; green line: DPPG; blue line: DSPG; cyan area: DOPG. (For interpretation of the references to color in this figure legend, the reader is referred to the web version of this article.)

**Table 3**
The average coordination number of carboxyl oxygen ($O_C$) and phosphoryl oxygen ($O_P$) atoms with respect to water hydrogens ($H_W$), sodium cations and guanidinium hydrogens ($H_G$), respectively. The first four lines refer to pure monolayers shown as the second number in each cell. In all systems the area per lipid was equal to 80 Å$^2$.

| $n_c$ | DLPG | DMPG | DPPG | DSPG | DOPG |
|---|---|---|---|---|---|
| $O_C$-$H_W$ | 0.881 | 0.909 | 0.939 | 0.890 | 0.920 |
| | 0.953 | 0.939 | 0.950 | 0.941 | 0.945 |
| $O_P$-$H_W$ | 1.908 | 1.946 | 1.926 | 1.947 | 1.928 |
| | 2.151 | 2.141 | 2.144 | 2.151 | 2.156 |
| $O_C$-$Na^+$ | 0.079 | 0.085 | 0.081 | 0.093 | 0.087 |
| | 0.111 | 0.121 | 0.121 | 0.119 | 0.109 |
| $O_P$-$Na^+$ | 0.069 | 0.064 | 0.061 | 0.070 | 0.073 |
| | 0.112 | 0.108 | 0.108 | 0.108 | 0.108 |
| $O_C$-$H_G$ | 0.050 | 0.036 | 0.031 | 0.042 | 0.039 |
| $O_P$-$H_G$ | 0.255 | 0.247 | 0.257 | 0.209 | 0.249 |

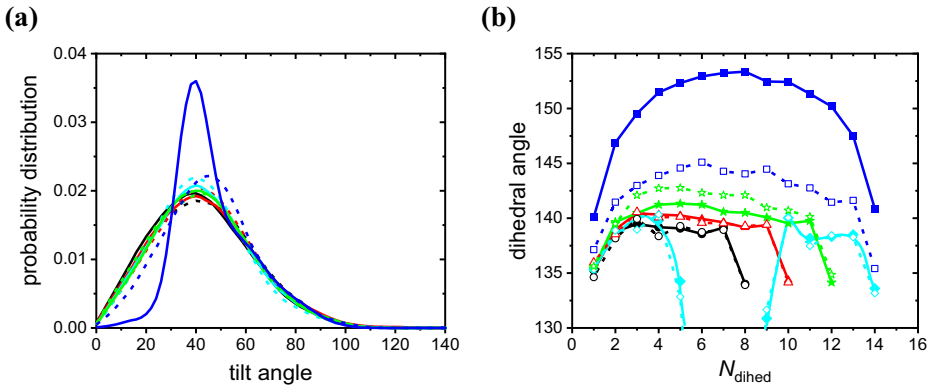


**Fig. 7.** Tilt angle probability distribution of *sn*-2 chains (a) and the average dihedral angles along *sn*-2 chains. The solid and dashed lines as well as the filled and empty symbols for panel (b) correspond to lipid monolayers with and without CX1 cations, respectively. DLPG (black); DMPG (red); DPPG (green); DSPG (blue); DOPG (cyan). Dihedral angles are measured from C-2 carbon atoms. (For interpretation of the references to color in this figure legend, the reader is referred to the web version of this article.)

## 4. Conclusions

The interaction of CX1 with phosphoglycerols used in this work was different depending on the hydrophobic chain structure. Among the five phosphoglycerols used, namely DLPG, DMPG, DPPG, DSPG and DOPG, the latter showed the least important increase of the molecular area and the least important change of the compressibility (compression experiments), the lowest increase of the surface pressure (adsorption experiments) and the least significant decrease of chain ordering and liquefaction of the monolayer (PM-IRRAS) in the presence of CX1. These unexpected results were interpreted in terms of the lowest affinity of CX1 for the unsaturated phosphoglycerol.

The compression and adsorption experiments indicate that below 30 mN $m^{-1}$ CX1 is intercalated between DSPG molecules; above this value it is progressively removed from the monolayer. The same process takes place with DPPG above 40 mN $m^{-1}$. In the case of DLPG and DMPG, CX1 is intercalated between the lipid molecules at all surface pressures. These proposals are supported by the adsorption results. The PM-IRRAS spectra obtained with DPPG or DSPG on the CX1 subphase at $\Pi$ = 60 mN·$m^{-1}$ reveal that CX1 is removed from the DPPG and DSPG monolayers at high surface pressures. The latter outcome is in accordance with the compression isotherm results as well.

The theoretical studies allowed understanding of the mechanism of lipid differentiation by CX1 observed experimentally. Molecular modeling showed that introduction of CX1 into the DOPG monolayers is the least favorable in terms of the free energy cost compared to the other lipids. Another important observation was that the number of CX1 transferred to the hydrophobic core region of the monolayer occurs with different efficiency depending on the structure of the hydrophobic tail. Indeed, three CX1 cations were observed in the DLPG tail region and only one in the case of DSPG. Importantly, there were no CX1 cations in the tail region of the DOPG monolayer. Another observation is the decrease of the chain ordering in the immediate vicinity of the CX1 cations. This is particularly well seen with longer chains.

As proposed before [14], the transfer of the CX1 cation from water to the tail region in the negatively charged phospholipids with myristoyl chains (DMPG or DMPS) is associated with a flip-flop movement of the calixarene crown and formation of CX1-phospholipid adducts. The results obtained in the present work indicate that the apolar interaction between CX1 and the lipid side chains can stabilize the adducts only when the chains adopt appropriate conformations. This situation occurs more easily in the phosphoglycerols with medium length chains (lauroyl or myristoyl) compared to the long chains (palmitoyl or stearoyl). Obviously, the double bond present in the oleoyl chains hampers conformations stabilizing the CX1-phospholipid adducts. This result indicates that new antibiotic structures capable of adjusting apolar interaction with lipid membranes may be needed. The latter concerns in particular the interaction with unsaturated lipids which are present in biological membranes.

## CRediT authorship contribution statement

**Beata Korchowiec:** Conceptualization, Methodology, Investigation, Data curation, Writing–original draft, Supervision, Funding acquisition. **Monika Orlof-Naturalna:** Investigation. **Jacek Korchowiec:** Software, Methodology. **Jean-Bernard Regnouf de Vains:** . **Maxime Mourer:** . **Ewa Rogalska:** .

## Declaration of Competing Interest

The authors declare that they have no known competing financial interests or personal relationships that could have appeared to influence the work reported in this paper.

## Acknowledgements

This work was supported by the project No. 2012/07/B/ST5/00890 from the Polish National Science Centre. Calculations were performed at Jagiellonian University, Faculty of Chemistry, on the PL-Grid infrastructure at ACK CYFRONET within the framework of the "HPC Infrastructure for Grand Challenges of Science and Engineering" project. The technical assistance of Małgorzata Kuniewicz and Eliza Kachnic is gratefully acknowledged.

## Appendix A. Supplementary data

Supplementary data to this article can be found online at https://doi.org/10.1016/j.molliq.2021.117636.

## References

[1] M.T. Blanda, J. Am. Chem. Soc. 129 (2007) 6963.
[2] D.M. Roundhill, Elsevier Ltd. (2004) 485–491.
[3] D.A. Fayzullin, N.N. Vylegzhanina, O.I. Gnezdilov, V.V. Salnikov, A.V. Galukhin, I.I. Stoikov, I.S. Antipin, Y.F. Zuev, Appl. Magn. Reson. 40 (2011) 231.
[4] M. Mourer, H.M. Dibama, S. Fontanay, M. Grare, R.E. Duval, C. Finance, J.-B. Regnouf-de-Vains, Bioorg. Med. Chem. 17 (2009) 5496.
[5] B. Korchowiec, J. Korchowiec, M. Gorczyca, J.-B. Regnouf de Vains, E. Rogalska, J. Phys. Chem. B 119 (2015) 2990.

[6] B. Korchowiec, A. Ben Salem, Y. Corvis, J.-B. Regnouf de Vains, J. Korchowiec, E. Rogalska, J. Phys. Chem. B 111 (2007) 13231.
[7] M. Mourer, R.E. Duval, C. Finance, J.-B. Regnouf-de-Vains, Bioorg. Med. Chem. Lett. 16 (2006) 2960.
[8] M. Grare, M. Mourer, S. Fontanay, J.-B. Regnouf-de-Vains, C. Finance, R.E. Duval, J. Antimicrob. Chemother. 60 (2007) 575.
[9] M. Grare, H.M. Dibama, S. Lafosse, A. Ribon, M. Mourer, J.B. Regnouf-de-Vains, C. Finance, R.E. Duval, Clin. Microbiol. Infect. 16 (2010) 432.
[10] M. Grare, E. Dague, M. Mourer, J.B. Regnouf-de-Vains, C. Finance, J.F.L. Duval, R. E. Duval, F. Gaboriaud, Pathol. Biol. 55 (2007) 465.
[11] M. Grare, S. Fontanay, H. Massimba Dibama, M. Mourer, J.B. Regnouf-de-Vains, C. Finance, R.E. Duval, Pathol. Biol. 58 (2010) 46.
[12] K.A. Brogden, Nat. Rev. Microbiol. 3 (2005) 238.
[13] R.F. Epand, P.B. Savage, R.M. Epand, Biochim. Biophys. Acta, Biomembr. 1768 (2007) 2500.
[14] G. Sautrey, M. Orlof, B. Korchowiec, J.-B. Regnouf de Vains, E. Rogalska, J. Phys. Chem. B 115 (2011) 15002.
[15] B. Korchowiec, M. Gorczyca, E. Rogalska, J.-B. Regnouf-de-Vains, M. Mourer, J. Korchowiec, Soft Matter 12 (2016) 181.
[16] R.G. Upchurch, Biotechnol. Lett. 30 (2008) 967.
[17] M.F. Siliakus, J. van der Oost, S.W.M. Kengen, Extremophiles 21 (2017) 651.
[18] R.M. Epand, R.F. Epand, Biochim. Biophys. Acta, Biomembr. 1788 (2009) 289.
[19] D. Saeloh, V. Tipmanee, K.K. Jim, M.P. Dekker, W. Bitter, S.P. Voravuthikunchai, M. Wenzel, L.W. Hamoen, PLoS Pathog. 14 (2018) 1006876.
[20] J. Beranova, M. Jemiola-Rzeminska, D. Elhottova, K. Strzalka, I. Konopasek, Biochim. Biophys. Acta, Biomembr. 1778 (2008) 445.
[21] A.W. Kingston, C. Subramanian, C.O. Rock, J.D. Helmann, Mol. Microbiol. 81 (2011) 69.
[22] A. Mueller, M. Wenzel, H. Strahl, F. Grein, T.N.V. Saaki, B. Kohl, T. Siersma, J.E. Bandow, H.-G. Sahl, T. Schneider, L.W. Hamoen, Proc. Natl. Acad. Sci. U. S. A. 113 (2016) 7077.
[23] M. Wenzel, N.O.E. Vischer, H. Strahl, L.W. Hamoen, Bio-Protoc. 8 (2018) 3063.
[24] L. Caseli, T.M. Nobre, A.P. Ramos, D.S. Monteiro, M.E.D. Zaniquelli, A.C.S. Symp, Ser. 1215 (2015) 65.
[25] G. Brezesinski, H. Mohwald, Adv. Colloid Interface Sci. 100–102 (2003) 563.
[26] J. Gravier, B. Korchowiec, R. Schneider, E. Rogalska, Chem. Phys. Lipids 158 (2009) 102.
[27] B.M. Korchowiec, T. Baba, H. Minamikawa, M. Hato, Langmuir 17 (2001) 1853.
[28] M. Girardon, B. Korchowiec, J. Korchowiec, E. Rogalska, N. Canilho, A. Pasc, J. Mol. Liq. 308 (2020) 113040.
[29] M. Gorczyca, B. Korchowiec, J. Korchowiec, S. Trojan, J. Rubio-Magnieto, S.V. Luis, E. Rogalska, J. Phys. Chem. B 119 (2015) 6668.
[30] O. Freudenthal, F. Quiles, G. Francius, K. Wojszko, M. Gorczyca, B. Korchowiec, E. Rogalska, Biochim. Biophys. Acta, Biomembr. 1858 (2016) 2592.
[31] J.T. Davies, E.K. Rideal, Interfacial Phenomena, 2nd ed., Academic Press, 1963.
[32] E. Darve, D. Rodriguez-Gomez, A. Pohorille, J. Chem. Phys. 128 (2008) 144120.
[33] J.C. Phillips, R. Braun, W. Wang, J. Gumbart, E. Tajkhorshid, E. Villa, C. Chipot, R. D. Skeel, L. Kale, K. Schulten, J. Comput. Chem. 26 (2005) 1781.
[34] J. Henin, G. Fiorin, C. Chipot, M.L. Klein, J. Chem. Theory Comput. 6 (2010) 35.
[35] J.B. Klauda, R.M. Venable, J.A. Freites, J.W. O'Connor, D.J. Tobias, C. Mondragon-Ramirez, I. Vorobyov, A.D. MacKerell Jr., R.W. Pastor, J. Phys. Chem. B 114 (2010) 7830.
[36] K. Vanommeslaeghe, E. Hatcher, C. Acharya, S. Kundu, S. Zhong, J. Shim, E. Darian, O. Guvench, P. Lopes, I. Vorobyov, A.D. Mackerell Jr., J. Comput. Chem. 31 (2010) 671.
[37] W.L. Jorgensen, J. Chandrasekhar, J.D. Madura, R.W. Impey, M.L. Klein, J. Chem. Phys. 79 (1983) 926.
[38] T. Darden, D. York, L. Pedersen, J. Chem. Phys. 98 (1993) 10089.
[39] D. Marsh, Biochim. Biophys. Acta, Rev. Biomembr. 1286 (1996) 183.
[40] M. Dyck, A. Kerth, A. Blume, M. Loesche, J. Phys. Chem. B 110 (2006) 22152.
[41] X. Bi, C.R. Flach, J. Perez-Gil, I. Plasencia, D. Andreu, E. Oliveira, R. Mendelsohn, Biochemistry 41 (2002) 8385.
[42] W. Hubner, A. Blume, Chem. Phys. Lipids 96 (1998) 99.
[43] M. Allouche, S. Castano, D. Colin, B. Desbat, B. Kerfelec, Biochemistry 46 (2007) 15188.
[44] S.J. Slater, C. Ho, F.J. Taddeo, M.B. Kelly, C.D. Stubbs, Biochemistry 32 (1993) 3714.
[45] A. Kundu, P.K. Verma, J.-H. Ha, M. Cho, J. Phys. Chem. A 121 (2017) 1435.
[46] H.L. Casal, H.H. Mantsch, H. Hauser, Biochemistry 26 (1987) 4408.
[47] H. Binder, G. Kohler, K. Arnold, O. Zschornig, Phys. Chem. Chem. Phys. 2 (2000) 4615.
[48] A. Stachowicz-Kusnierz, S. Trojan, L. Cwiklik, B. Korchowiec, J. Korchowiec, Chem. - Eur. J. 23 (2017) 5307.